Check for updates

Received: 12 January 2021 | Revised: 9 February 2021 | Accepted: 11 February 2021

DOI: 10.1002/syn.22197

RESEARCH ARTICLE

SYNAPSE WILEY

Suppression of food restriction-evoked hyperactivity in activity-based anorexia animal model through glutamate transporters GLT-1 at excitatory synapses in the hippocampus

Olesia M. Bilash[1,2] | Hannah S. Actor-Engel[2] | Ang D. Sherpa[2] | Yi-Wen Chen[2] | Chiye Aoki[1,2]

[1]The Neuroscience Institute, NYU Langone Medical Center, New York, NY, USA

[2]Center for Neural Science, New York University, New York, NY, USA

Correspondence
Chiye Aoki, Center for Neural Science, New York University, New York, NY 10003, USA.
Email: ca3@nyu.edu

Funding information
National Eye Institute; National Science Foundation; NIH, Grant/Award Number: R21MH105846; Klarman Family Foundation Grant Program in Eating Disorders Research, Grant/Award Number: P30 EY13079; New York University Research Challenge Fund; NSF-REU; The Vulnerable Brain Project

Abstract

Severe voluntary food restriction is the defining symptom of anorexia nervosa (AN), but anxiety and excessive exercise are maladaptive symptoms that contribute significantly to the severity of AN and which individuals with AN have difficulty suppressing. We hypothesized that the excitability of hippocampal pyramidal neurons, known to contribute to anxiety, leads to the maladaptive behavior of excessive exercise. Conversely, since glutamate transporter GLT-1 dampens the excitability of hippocampal pyramidal neurons through the uptake of ambient glutamate and suppression of the GluN2B-subunit containing NMDA receptors (GluN2B-NMDARs), GLT-1 may contribute toward dampening excessive exercise. This hypothesis was tested using the mouse model of AN, called activity-based anorexia (ABA), whereby food restriction evokes the maladaptive behavior of excessive wheel running (food restriction-evoked running, FRER). We tested whether individual differences in ABA vulnerability of mice, quantified based on FRER, correlated with individual differences in the levels of GLT-1 at excitatory synapses of the hippocampus. Electron microscopic immunocytochemistry (EM-ICC) was used to quantify GLT-1 levels at the excitatory synapses of the hippocampus. The FRER seen in individual mice varied more than 10-fold, and Pearson correlation analyses revealed a strong negative correlation ($p = .02$) between FRER and GLT-1 levels at the axon terminals of excitatory synapses and at the surrounding astrocytic plasma membranes. Moreover, synaptic levels of GluN2B-NMDARs correlated strongly with GLT-1 levels at perisynaptic astrocytic plasma membranes. There is at present no accepted pharmacotherapy for AN, and little is known about the etiology of this deadly illness. Current findings suggest that drugs increasing GLT-1 expression may reduce AN severity through the reduction of GluN2B-NMDAR activity.

KEYWORDS

anorexia nervosa, anxiety, exercise, GluN2B, hyperactivity

 © 2021 Wiley Periodicals, Inc.

1 | INTRODUCTION

Anorexia nervosa (AN) is an eating disorder accompanied by stress-induced anxiety (Dellava et al., 2010; Kaye et al., 2004) and compulsive, excessive exercise (Beadle et al., 2015; Davis et al., 1999; Kron et al., 1978; Thornton et al., 2011; Watson et al., 2019; Zunker et al., 2011). These behavioral traits combine with voluntary food restriction (Thornton et al., 2011), leading to severe weight loss and even death (Arcelus et al., 2011; Birmingham et al., 2005; Sullivan, 1995). AN has the highest death rate of any psychiatric illness, even surpassing the mortality associated with major depression (Arcelus et al., 2011). Currently, there are no FDA-approved pharmacotherapy treatment options for AN, and little is known about the etiology of this deadly illness (Hermens et al., 2020).

The rodent model, activity-based anorexia (ABA), has been useful for investigating the neurobiological bases of AN (Aoki et al., 2017; Casper et al., 2008; Gutierrez, 2013; Hebebrand et al., 2003). This model utilizes the wheel acclimation-plus-food restriction regimen (described in greater detail under "Methods"). Using the mouse ABA model, we have shown that hungry adolescent wild-type mice, like individuals diagnosed with AN, voluntarily food-restrict, in that they choose to over-exercise on wheels, even during the limited hours of food availability (Chowdhury et al., 2013). Even though food restriction alone never causes death, some mice that have undergone ABA induction will die unless carefully monitored. In this way, ABA captures one of the general agreements about AN — its high mortality rate. One idea as to why hungry animals exhibit food restriction-evoked running (FRER) is that it is an innate behavior, simulating foraging behavior (Carr, 2011; Casper et al., 2008; Gutierrez, 2013). However, FRER measurements reveal that, even if innate, the *extent* to which food-restricted adolescents run differs greatly across individuals. The *change* in anxiety, assessed by comparing the anxiety level before food restriction (FR), (using the open field test, and after food restriction, using the elevated plus-maze test, correlates strongly with individual differences in FRER (Wable et al., 2015).

The emergence of AN and other anxiety disorders are most prevalent during adolescence. Adolescence may be a particularly vulnerable developmental stage for AN and other mental illnesses, due to transient mismatches in the maturation of interconnected brain regions (Goddings et al., 2014; Mills et al., 2014). Unlike sensory neocortices, the hippocampus (HPC) receives multisensory input from various neocortical areas and undergoes robust developmental changes during adolescence (Chen, Akad, et al., 2018; Chowdhury, Barbarich-Marsteller, et al., 2014; Chowdhury, Rios, et al., 2014). The dorsal HPC is well-recognized for its role in spatial cognition (Fanselow & Dong, 2010; Shen et al., 2010), but together with the ventral HPC, the dorsal HPC also participates in anxiety regulation (Huttunen & Myers, 1986; Kataoka et al., 1991; Shen et al., 2007; Talaenko, 1993). Both the dorsal and ventral HPC undergo robust expansion, then pruning of dendritic arbors throughout adolescence (Chen, Akad, et al., 2018).

Genome-wide association studies (GWAS) have revealed genetic linkages between AN and single-nucleotide polymorphisms (SNPs) of genes encoding intercellular adhesions, which are expressed at especially high levels in pyramidal neurons in the HPC CA1 field (Watson et al., 2019). These studies suggested to us that analysis of intercellular contacts (neuron-glia and synaptic contacts) in the adolescent HPC may provide insights regarding the etiology of AN. This idea also stems from our previous data showing that ABA induction during adolescence increases the levels of postsynaptic GluN2B-subunits of NMDA receptors (GluN2B-NMDAR) in the dorsal HPC, especially among individuals exhibiting the most severe weight loss (Chen et al., 2017). Conversely, GABAergic synapses in the dorsal HPC are strengthened the most among the ABA-induced individuals showing minimal FRER, suggesting that dampening hippocampal excitability could be protective against ABA vulnerability by suppressing FRER (Aoki et al., 2012, 2014, 2017; Chen, Actor-Engel, et al., 2018).

In this study, we analyzed the putative participation of glutamate transporter GLT-1 in the HPC in ABA vulnerability. There are multiple isoforms of glutamate transporters engaged in the uptake of extracellular glutamate. Most isoforms are expressed only by astrocytes, but GLT-1 is also expressed at the plasma membranes of axon terminals forming excitatory synapses in the CA1 field, as shown by our earlier EM-ICC data (Chen et al., 2004; Petr et al., 2015). The plasma membranes of astrocytic processes are often immediately juxtaposed to presynaptic axons, postsynaptic spines, or both (Ventura & Harris, 1999), and these astrocytic processes also express GLT-1 (Chen et al., 2004; Petr et al., 2015). Extracellular glutamate uptake by glutamate transporters has long been recognized to be important for preventing excitotoxicity (Danbolt, 2001; Danbolt et al., 2016). This includes contributions by GLT-1 (Petr et al., 2015; Rothstein et al., 1996). GLT-1 may also participate in synaptic plasticity (Barnes et al., 2020) and modulation of behavior, including the prevention of pathologically-repetitive grooming behaviors (Kanarek et al., 2009) and cocaine relapse (Knackstedt et al., 2010). Thus, in this study, we asked whether vulnerability to ABA, quantified based on FRER values, correlates with GLT-1 levels at excitatory synapses in the CA1 field of HPC. We used EM-ICC to assess GLT-1 levels. Because GLT-1 has been reported to aid as an anti-depressant by modulating the ketamine-sensitive GluN2B-NMDAR currents (Miller et al., 2014), we also used dual EM-ICC to assess the location of GLT-1 relative to the GluN2B-NMDARs at axo-spinous synapses of the CA1 field.

2 | METHODS

2.1 | Induction of ABA

All procedures involving the use of live animals were conducted according to NIH guidelines and the Institutional Animal Care and Use Committee at New York University (Animal Welfare Assurance No. A3317-01). Approximately 80% of mid-adolescent mice exhibit day-by-day

increases in wheel running when they are first acclimated to the wheel for a few days under the condition of *ad libitum* food (postnatal day (P) 36–40), and then experience limited food access (Chowdhury et al., 2013). Their FRER continues even during the limited hours of food availability (7 p.m. to 9 p.m., P41–P44). This behavior of continuing to run, in face of hunger and food availability, contributes greatly to weight loss. In contrast, when the same animals are re-acclimated to the wheel for the second time from P50, only about 50% of the animals exhibit FRER, with the remaining animals exhibiting suppression of wheel running, in spite of still losing weight due to limited food access (Chowdhury et al., 2013). Thus, the imposition of two bouts of ABA reveals greater individual differences in vulnerability to ABA, compared to one bout of ABA, quantified as the extent of FRER during the first and second ABA (ABA1, ABA2) and change in FRER between ABA1 and ABA2. In this study, we took advantage of the individual differences in vulnerability to ABA to ask whether these differences in behavior correlate with individual differences in GLT-1 levels at excitatory synapses in the CA1 field of HPC.

C57BL6/J mice were bred and reared at NYU's animal facility, with lights on from 7 a.m. to 7 p.m. (12 hr light:12 hr dark). Eight such female adolescent mice were used for the current study that underwent two bouts of ABA induction—ABA1 and ABA2—with 6 days of recovery, then of re-acclimation to the wheel without food restriction for 4 days in between. The food-restricted period was 3 days for ABA1 (typically P41–P44), because any longer period would result in mortality. During the recovery period, (typically P44–P50), animals had no access to the wheel and food was available *ad libitum*. These animals were then re-acclimated to the wheel for 4 days, typically from P50–P54, and then entered ABA2. For ABA2, typically spanning P54–P58, the food-restricted period was lengthened to 4 days, since animals could tolerate longer duration of food restriction without dying (Chen et al., 2016; Chowdhury et al., 2013; Wable et al., 2015). This schedule is schematized in Figure 1. The actual postnatal days varied by ±1 day, so as to combine litters born on different days.

In addition to the ABA-induced mice, the body weights of 12 female mice, ages P36 to P58 and with half of them having access to a wheel, were measured to assess whether ABA-induced animals regained weight during recovery to the extent comparable to those without the experience of food restriction.

From our previous studies, we noted that mice exhibit individual differences in their preference for food, with some preferring wet food (Clear H_2O DietGel 76A, 99.8 kcal per 100 g), while others consistently prefer the standard dry food (PMI Mouse Diet 5001, 335 kcal per 100 g) (Chowdhury et al., 2015; Smits et al., 2008). To avoid food neophobia (Kronenberger & Medioni, 1985), both wet food and dry chow were made available to animals from the day of weaning.

2.2 | Wheel running measurements

Wheel running measurements were made using the ENV-044 Low-Profile Mouse Wheel system (Med Associates, Inc., St. Albans, VT), for which 2,654.86 wheel turns equals 1 km of running distance. Wheel running measurements were made continuously from P36 to P60, except for the 6 days of recovery between ABA1 and ABA2. Wheel activity during the 2 days preceding ABA1 and ABA2 were averaged to determine each animal's baseline wheel activity.

FRER was determined for each animal, calculated as the increase of averaged daily wheel activity during the 3 days of food restriction above the baseline of ABA1 and during the 4 days of FR of ABA2, above the baseline of ABA2. The change in FRER from ABA1 to ABA2 was calculated by subtracting FRER during ABA2 from FRER of ABA1.

2.3 | Body weight and food consumption measurements

These measurements were made daily from P36 to P60. On days without food restriction, the measurements were made once per day, during the light hours. On the first day of food restriction of ABA1 and ABA2, measurements were made three times: at 1 p.m. just prior to removing food, at 7 p.m. just prior to the start of the feeding period, and at 9 p.m., immediately following the feeding period. On subsequent food restriction days, measurements were made twice—at 7 p.m. and 9 p.m.

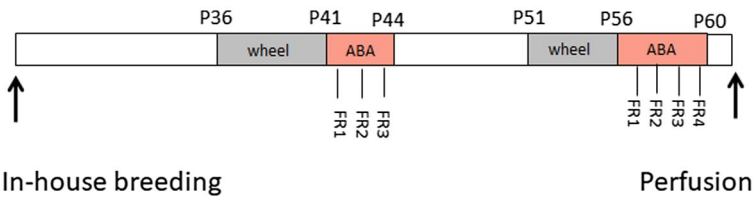

FIGURE 1 Timeline of the ABA-induction paradigm. All animals were singly housed, fed *ad libitum*, and underwent two cycles of ABA as described under "Methods." ABA1 consisted of three days of food restriction—FR1, FR2, and FR3. ABA2 consisted of 4 days of food restriction—FR1 through FR4. Animals were euthanized by transcardial perfusion with aldehydes 1 to 2 days after ABA2 ended

2.4 | preparation for EM-ICC

Within 2 days of the last day of ABA2, animals were deeply anesthetized using Urethane (1,200 mg/kg, intraperitoneal), then euthanized by transcardial perfusion with aldehydes as described previously (Chowdhury et al., 2013). In brief, animals were transcardially perfused first with 12.5 ml of phosphate-buffered saline (PBS) (0.01 M phosphate buffer and 0.9% NaCl, pH 7.4) containing 20 U/ml of Heparin, then with 250 ml of 0.1 M phosphate buffer (PB) containing 4% paraformaldehyde (pH 7.4), using a peristaltic pump set at a flow rate of 25 ml/min. Upon removing the brains from the skulls, the brains were post-fixed by immersion in a solution consisting of 4% paraformaldehyde and 0.1 M PB for 2 days at room temperature, followed by a minimum of 1 week in the cold room at 4°C. Coronal vibratome sections, set at a thickness of 50 μm and containing the HPC were stored at 4°C in the buffer consisting of PBS and 0.05% sodium azide (PBS-azide) for up to 1 week. Of the eight brains harvested, only seven were preserved adequately by transcardial perfusion with fixatives. Thus, brains of seven of these eight animals were processed for the EM-ICC detection of GLT-1 and GluN2B subunits of NMDARs.

2.5 | Information of antibodies used for EM-ICC

The mouse monoclonal anti-GLT-1 (RRID:AB_2314565) was generously provided by the laboratory of Dr. J. D. Rothstein (Johns Hopkins Univ.). The original concentration of anti-GLT-1a was 6.7 mg/ml. This antibody was previously shown to be specific at a dilution of 1:10,000 for detecting neuronal and astrocytic profiles, based on the elimination of immunolabeling within neuronal processes of hippocampal, striatal, and cortical tissue following global and neuron-specific genetic deletion of GLT-1 in mice (Churchill et al., 2002; Greenwood & Fleshner, 2008; Petr et al., 2015) and by the elimination of immunolabeling within astrocytic processes following the astrocyte-specific genetic deletion of GLT-1 in mice (Petr et al., 2015).

The rabbit antibody directed against the GluN2B subunit of NMDA receptors was purchased from Upstate Biotechnology (RRID:AB_310193, Catalog No. 06-600, distributed by Millipore), This antibody identifies GluN2B subunit C's terminal amino acids 1,437–1,456 (KFNGSSNGHVYEKLSSIESDV). The antibody was previously demonstrated to be mono-specific by Western blotting, based on the immunoreactivity of a single 180 kD band from rat brain microsomal preparation, corresponding to the predicted molecular weight for the GluN2B subunit based on its amino acid sequence. Moreover, this antibody does not recognize NR1 or NR2A subunits of the NMDA receptor (Rinaldi et al., 2007). At a dilution of 1:40, the antibody recognizes asymmetric synapses but not symmetric synapses (Aoki, Lee, et al., 2009; Fujisawa & Aoki, 2003). This antibody has been used to characterize postnatal changes in the level of GluN2B-containing NMDARs at asymmetric synapses of the visual cortex. The developmental profile has been described previously by Western blot experiments (Services, 1998). Namely, there is a greater prevalence of GluN2B subunits within younger forebrain tissue than in mature tissue, thereby differing significantly from the developmental profile of NR2A immunoreactivity (Paluska & Schwenk, 2000).

The secondary antibody used for detecting GLT-1 was donkey anti-mouse IgG, conjugated to 0.8 nm colloidal gold particles (Electron Microscopic Sciences, Hatfield PA, Catalog No. 25811).

The secondary antibody used for detecting NMDAR subunits was donkey anti-rabbit IgG conjugated to 10 nm colloidal gold particles (Electron Microscopic Sciences, Hatfield, PA, Catalog No. 25705).

2.6 | GLT-1 EM-ICC by the silver-intensified gold (SIG) procedure

GLT-1 EM-ICC was performed using the anti-GLT-1 antibody and detection of immunolabeling by the SIG procedure, as described previously (Aoki et al., 2014).

Briefly, vibratome sections were first incubated in mouse anti-GLT-1 antibody at a dilution of 1:10,000, using PBS-azide containing 1% bovine serum albumin (PBS-BSA-Azide) overnight under constant agitation at room temperature. Following three rinses in PBS to remove excess unbound primary antibodies, the vibratome sections were incubated in the secondary antibody comprised of donkey anti-mouse IgG conjugated to 0.8 nm colloidal gold at a dilution of 1:100 using PBS-BSA-azide as the diluent. Following three rinses in PBS to remove excess unbound secondary antibodies, the vibratome sections were post-fixed with 2% glutaraldehyde, buffered with PBS using spot wells. After fixation for 30 min at room temperature, sections were rinsed in PBS over a 15 min period, then in 0.1 M citrate buffer (pH 6.0) for 1 min, then reacted with the silver-intensification kit (KPL, SeraCare) for 25 min at room temperature to enlarge colloidal gold particles conjugated to the secondary antibody. The silver-intensification step was terminated by rinsing vibratome sections for 1 min in 0.1 M citrate buffer, then returned to PBS. The sections were processed for ultrastructural preservation and contrast enhancement, using Phend's protocol for osmium-free tissue processing for EM and post-embed immunogold labeling (PEG), which involved reacting the vibratome sections with tannic acid, iridium tetrabromide, and uranyl acetate (Phend et al., 1995). Ultrathin sections oriented tangentially to the vibratome section surfaces were

prepared at a thickness of 70–100 nm using an ultramicrotome (MT-7, RMC Boeckeler, Tucson, AZ) and collected on nickel grids (400 thin-bar mesh, Electron Microscopy Sciences, Catalog No. 15800). Ultrathin sections were counterstained with Reynold's lead citrate for 10–20 s.

EM images were captured at a magnification of 40,000x using a transmission EM model JEOL within the stratum radiatum of the CA1 field of dorsal HPC. Image capturing was achieved by the AMT digital camera system with the Hamamatsu XR80 CCD camera (Woburn, MA). Each micrograph contained zones lacking neuropil (i.e., the embedding matrix without tissue), to ensure that the surface-most regions of vibratome sections were sampled, where the reactivity of tissue with immunoreagents would be optimal. Otherwise, image capturing was kept random. Random sampling was achieved by scanning the neuropil area systematically, from left to right, then down, then right to left across the neuropil area bordered by grid squares, while avoiding to sample any excitatory synapse more than once, until 100 excitatory axo-spinous synapses were encountered. Table 1 lists the number of electron micrographs and neuropil area that were required to capture images of 100 excitatory axo-spinous synapses. Experimenters were kept blind to animals' behavioral characteristics.

Astrocytes were identified by their irregular concave contours that immediately abutted convex dendritic spines and axon terminals (Ventura & Harris, 1999). Astrocytic processes exhibiting immediate juxtapositions with any part of the dendritic spine or axon terminal, or lateral to the synaptic cleft of axo-spinous excitatory synapses with thick postsynaptic densities (PSDs), were categorized as "synaptically associated astrocytic processes." The location of SIG particles was recorded to be at one of the following mutually exclusive positions in relation to axo-spinous excitatory synapses with thick PSDs: presynaptic axon terminals; postsynaptic, within dendritic spines; astrocytic process adjacent to excitatory axo-spinous synapses, which we refer to as peri-synaptic; astrocytic processes without apparent juxtapositions to excitatory axo-spinous synapses within the plane of ultrathin section. For each of the four subcellular sites, the SIG particles were further categorized based on their position over the plasma membrane or located intracellularly (lacking detectable contact between the SIG particle and plasma membrane).

The identity of these fine structures was based on morphological characteristics described by Peters et al. (1991). Additionally, astrocytic processes were distinguished from microglial processes based on morphological criteria of Tremblay et al. (Mehl et al., 2000) and Sogn et al. (Smith & Lyle, 2006), who described microglia as exhibiting electron-dense cytoplasm, multiple vesicles, vacuoles, elongated endoplasmic reticulum, and rare contacts with synapses. Microglia have also been reported to express GLT-1 *in vivo* and in the HPC (Beschorner et al., 2007; Girbovan et al., 2016). Since we did not employ molecular markers to distinguish astrocytes from microglia, we acknowledge that some of the glial processes may not have been astrocytes.

2.7 | GluN2B-NMDAR EM-ICC by the PEG (post-embed gold) procedure

Localization of GluN2B-subunits of NMDARs was achieved by the PEG procedure. The vibratome sections that underwent immunocytochemical detection of GLT-1 were processed for the EM-ICC localization of GluN2B subunits, following the procedure described previously (Chen et al., 2017) and described briefly below, using a rabbit anti-GluN2B antibody, followed by incubation in a secondary antibody goat anti-rabbit IgG conjugated to 10-nm colloidal gold particles (Electron Microscopy Sciences).

Incubation with the primary antibody commenced within 3 hr of preparing ultrathin sections. Ultrathin sections were collected on formvar-coated 200-mesh grids. Ultrathin sections on grids were conditioned for 30 min in a buffer consisting of 0.1 M Tris-buffer (pH 7.6) with 0.9%

TABLE 1 Area sampled for EM-ICC

Animal ID	Color codes in Figures 4 and 5	Area sampled for GLT-1 EM-ICC (no. of micrographs)	Area sampled for NR2B EM-ICC (no. of micrographs)
239381	Blue	185 μm^2 (11)	285 μm^2 (38)
239384	Black	436 μm^2 (26)	270 μm^2 (36)
239369	Orange	202 μm^2 (12)	315 μm^2 (42)
239362	Red	336 μm^2 (20)	330 μm^2 (44)
239363	Olive	269 μm^2 (16)	330 μm^2 (44)
240279	Green	185 μm^2 (11)	270 μm^2 (36)
242018	Pink	269 μm^2 (16)	330 μm^2 (44)

Not<del author="Chiye Aoki" command="Delete" timestamp="1614534320818" title="Deleted by Chiye Aoki on 2/28/2021, 12:45:20 PM" class="reU3" id="edit85">e</del>: The table lists the total area scanned for each of the seven brains that underwent EM-ICC analysis. Typically, the electron micrographs used to analyze GLT-1 immunoreactivity contained zones lacking tissue, so as to ensure that neuropil sampling occurred along the surface-most regions of vibratome sections. The electron micrographs used to analyze GluN2B-immunoreactivity did not exclude zones occupied by large dendrites or somata. Since neither of these zones was subtracted to assess the synaptic neuropil area that was sampled, the individual differences in the areas sampled are not reflective of individual differences in synapse density.

NaCl and 0.1% Triton X-100 (TBST-7.6), then incubated overnight at room temperature in a small puddle of anti-GluN2B diluted to 1:40 (10 μg/ml) using the TBST-7.6 buffer. Evaporation of the antibody puddle was minimized by placing the grids on a silicone mat surrounded by water puddle within a petri dish chamber. On the following day, grids were rinsed two times using TBST-7.6, then conditioned with TBST with the pH adjusted to 8.2 (TBST-8.2) for 5 min, and then incubated for 1 hr at room temperature in TBST-8.2 in secondary antibody, i.e., goat-anti-rabbit IgG conjugated to 10 nm colloidal gold particles. Grids were rinsed three times using TBST-8.2, then in distilled water, then post-fixed for 10 min at room temperature using 1% glutaraldehyde diluted using distilled water. Grids were rinsed using distilled water, then counterstained for 10–20 s using Reynold's lead citrate. Control grids containing adjacent ultrathin sections underwent the exact same procedure, except that the overnight incubation in TBST-7.6 lacked the primary antibody.

In order to assess whether synaptic neuropil of CA1 stratum radiatum exhibited individual differences in GluN2B-subunit levels, excitatory synapses in stratum radiatum of dorsal HPC from vibratome sections that did not undergo GLT-1 EM-ICC were analyzed systematically for the presence of PEG particles, strictly in the order of encounter at a magnification of 60,000x, until the analyzed number of excitatory axo-spinous synapses reached 200 for each animal. As described for the GLT-1 immunolabeled samples, the analysis was undertaken for all synapses encountered, strictly in the order of encounter, as the microscopist scanned the neuropil by moving the sample from left to right, then down and then right to left, to avoid scanning the neuropil area more than once. The total number of micrographs and area of neuropil required to capture 200 axo-spinous synapses are indicated in Table 1.

The locations of PEG particles were recorded to be in one of the mutually exclusive positions, as depicted in Figure 2. The bin analysis of synaptic GluN2B was described previously (Aoki et al., 2003; Aoki, Kojima, et al., 2009; Aoki, Lee, et al., 2009; Chen et al., 2017; Fujisawa & Aoki, 2003) and is in close alignment with the pioneering work done by the laboratory of John H. Morrison (Adams et al., 2001; He et al., 1998) except that our counting included the extrasynaptic PEG particles that were anywhere along the spinous plasma membrane, rather than only ≤15 nm from the lateral edges of PSDs.

2.8 | Statistical analyses

Potential association between two measurements was assessed by the Pearson correlation analysis. To assess whether the group mean value of body weight differed significantly from the baseline value just prior to ABA1 and ABA2, the Wilcoxon Signed Rank Test was performed. For all analyses, p values < .05 were accepted as significant. The software, Prism (GraphPad v6 and 8) was used to perform the statistical analyses and graphs.

2.9 | Preparation of figures

Adobe Photoshop (version 2020) was used to crop, enlarge, alter contrast, alter the brightness, and annotate electron micrographs and graphs to create figures. These manipulations did not alter detectability of SIG or PEG labels, which were always of maximal opacity.

3 | RESULTS

3.1 | Increases in body weight during adolescence are disrupted by ABA

Female mice exhibit increases in body weight during adolescence when fed *ad libitum* (Chowdhury et al., 2013). However, within the first 6 hr of food restriction, all animals significantly decreased body weights relative to their baseline body weight measured at 1 p.m. on P41, as revealed by the Wilcoxon Signed Rank Test (Figure 3, FR1 of ABA1, p(two-tailed) = .008, N = 8). Although their body weights increased during the hours of food availability (7 p.m. to 9 p.m.), the food restriction from 9 p.m. to 7 p.m. of the next day (FR2 at P42) and subsequent days (FR3 at P43) led to further weight losses that were significant, relative to the baseline body weight measured at 1 p.m. on P41 (p = .008, N = 8 for FR2 and 3). Compared to age-matched female mice that were not food-restricted, ABA induction caused significant weight loss on P43 that could not be regained even after the 2 hr of food availability (p = .0049, t (16) = 4.688, Holm-Sidak method of multiple t tests; mean of non-FR group = 17.55 ± 0.56 g (N = 10); mean of ABA group = 14.17 ± 0.39 g (N = 8)).

When animals were re-exposed to food restriction during ABA2, starting at 1 p.m. on P53-P55 (FR1), animals again lost weight within the first 6 hr. However, this decrease did not reach statistical significance relative to baseline weight at 1 p.m. (Figure 3, Wilcoxon Signed Rank Test, p = .195, N = 8). As was observed during ABA1, animals regained weight during the 2 hr of feeding (7 p.m. and 9 p.m.) of FR1, but lost a significant amount of weight between 9 p.m. of FR1 and 7 p.m. of FR2 the next day (p = .008, N = 8). Weight losses accumulated significant

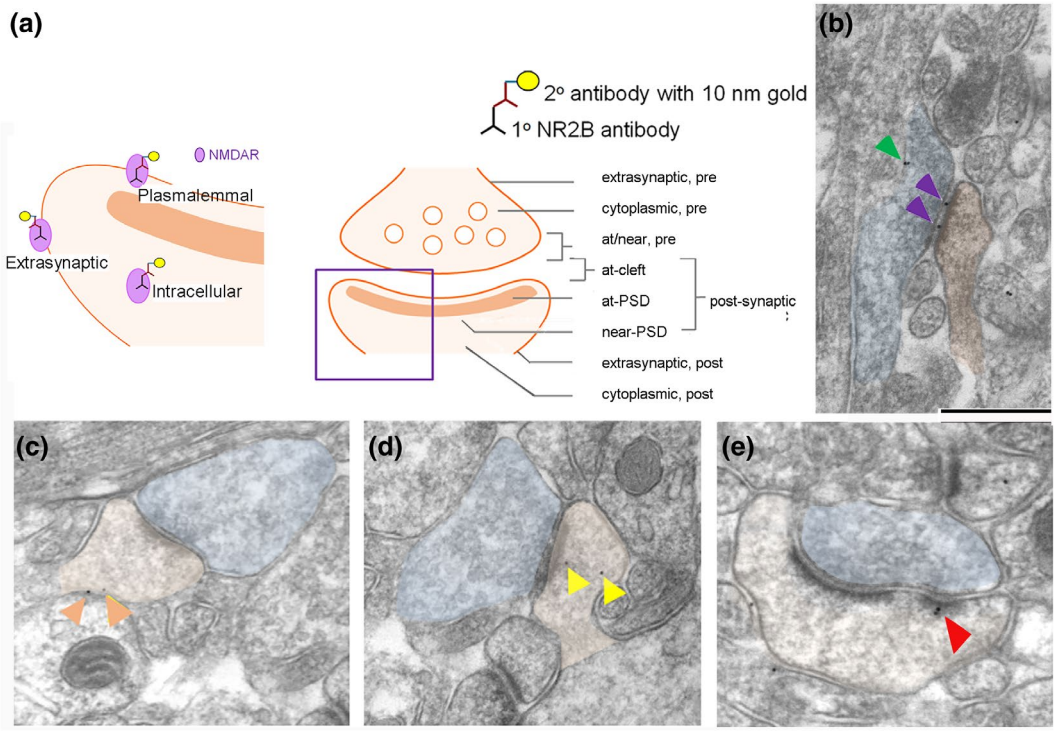

FIGURE 2 Categories of GluN2B-immunoreactive sites at axo-spinous synapses. (a) GluN2B subunits of NMDARs were localized using a primary (1°) antibody which, in turn, was recognized by a secondary (2°) antibody conjugated to 10-nm colloidal gold particles (PEG procedure). The antigenic site was identified to be plasmalemmal versus cytoplasmic, and synaptic versus extrasynaptic, at axo-spinous synapses. Extrasynaptic zones along the plasma membrane spanned regions that were more than 10 nm removed from the PSD along the postsynaptic spine's plasma membrane (extrasynaptic, post) or more than 10 nm removed from the active zone along the presynaptic axon terminal plasma membrane (presynaptic, pre). The location of PEG particles at postsynaptic sides was sub-categorized further as indicated in the cartoon. The electron micrographs show examples of labeling: (b) extrasynaptic labeling in the presynaptic terminal (green arrowhead); labeling in the synaptic cleft (purple arrowheads); (c) extrasynaptic labeling in the postsynaptic spine (orange arrowheads); (d) labeling near the PSD and cytoplasmic labeling within the postsynaptic spine (yellow arrowheads); and (e) labeling at the PSD in the postsynaptic spine (red arrowhead). Calibration bar equals 400 nm and applies to all electron micrographs. The electron micrographs were captured at a magnification of 60,000x

during the subsequent days, measured at 7 p.m. just prior to the feeding hours ($p = .008$ for FR3 and FR4, $N = 8$ for both comparisons), and the weights were not regained fully by the 2-hr feeding period, based on comparison of body weights at 9 p.m. ($p = .039$ for FR2, $p = .0156$ for FR3 and FR4).

3.2 | FRER varies widely across individuals

Average wheel running increased modestly in response to food restriction during ABA1, but none of the days reached statistical significance relative to the baseline running on the days before food restriction. This lack of significance in group averages of FRER (Figure 4a) was due to the large variance in the extent of FRER across individual animals. The FRER, averaged across the three food restriction days of ABA1, ranged from −4.8 km to 17 km/day, with six out of eight mice exhibiting FR-induced increases, and the remaining two mice exhibiting reductions (negative FRER values in Figure 4b). During ABA2, the average FRER varied even more, ranging from −8.2 to 25.4 km/day, with six mice exhibiting food restriction-induced increases and two mice exhibiting decreases (Figure 4b). Comparisons of FRERs between ABA1 and ABA2 indicated that three individuals reduced FRER during ABA2, relative to ABA1 by as much as 14 km/day, while five increased FRER by as much at 17 km/day ("Change in FRER," Figure 4b).

FRER during ABA1 was not a predictor of FRER during ABA2. For example, one animal exhibited the highest FRER during ABA1 but not during ABA2 (Figure 4b, red data point). Conversely, the animal with the lowest FRER during ABA1 increased its FRER much more than others, yielding the second highest increase in FRER (Figure 4b, green). Meanwhile, the animal exhibiting the greatest overall increase in FRER did not run particularly far during ABA1 (Figure 4b, purple).

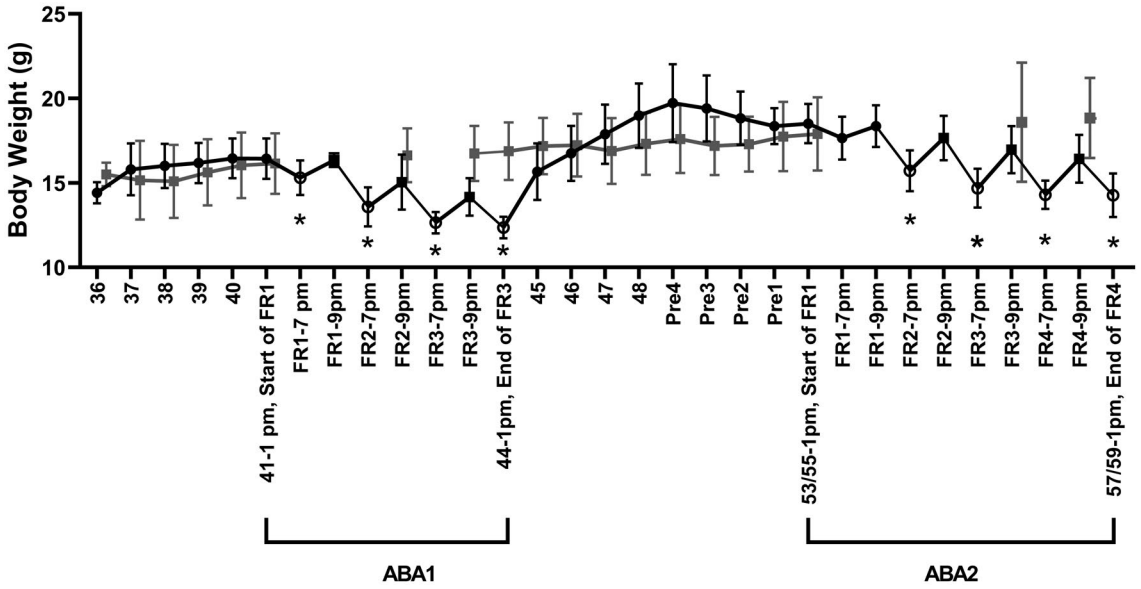

FIGURE 3 Body weight changes during ABA1 and ABA2. Daily values of group averages of body weight (in grams) are shown for animals that underwent two inductions of ABA (black). Body weights of age-matched females that did not undergo food restriction are shown for comparison, with and without wheel access (light grey). Error bars indicate *SEM*. For the ABA-induced group, body weight is significantly reduced following removal of food at 1 p.m. on P41, based on measurement at 7 p.m., 6 hr later. Although body weight increases during the 2 hr of food access (7 p.m. to 9 p.m.), body weight repeatedly and significantly drops from 9 p.m. to 7 p.m. of the next day. The four asterisks spanning ABA1 indicate significant differences at $p < .05$, relative to the baseline value measured at 1 p.m. on P41 of the ABA group. During recovery from ABA1, body weight is rapidly restored and resumes increasing, as expected, since animals are still adolescents. Re-acclimation to the wheel without food restriction begins on Pre4 (4 days before the onset of ABA2). For the first 6 hr of ABA2 (FR1), weight loss is not significantly altered. However, body weight decreases significantly from 9 p.m. to 7 p.m. on the following food restriction days (FR2, FR3, FR4). The four asterisks spanning ABA2 indicate significant differences from baseline, measured at 1 p.m., just before commencing FR1 of ABA2. Open circles highlight the body weights at the end of daily food-restricted periods

3.3 | GLT-1 immunoreactivity is evident at excitatory axo-spinous synapses and the immediately adjacent astrocytic processes

Excitatory axo-spinous synapses were readily identified in stratum radiatum of the dorsal HPC CA1 field, based on the prevalence of uniformly-shaped vesicles within the presynaptic axon terminal and on the thick PSDs on the plasma membrane of dendritic spines, which formed a parallel alignment with the presynaptic terminal membrane. Almost all of the excitatory axo-spinous synapses in stratum radiatum were immediately adjacent to astrocytic processes, either along the postsynaptic spine, presynaptic axon terminal, or both. SIG reflecting GLT-1 immunoreactivity was readily evident along the plasma membrane of synaptically associated astrocytic processes (Figure 5a). Astrocytic processes without apparent synaptic association also exhibited SIG. Axon terminals forming asymmetric synapses onto dendritic spines were also immunoreactive for GLT-1, with some of the SIG located intracellularly (Figure 5a). Dual immunolabeling for GLT-1 and GluN2B-subunit of NMDA receptors confirmed that these axo-spinous synapses with GLT-1 immunoreactivity were glutamatergic, based on the localization of GluN2B-NMDAR subunits at the postsynaptic membrane and in the synaptic cleft (Figure 5b).

3.4 | GLT-1 immunoreactivity correlates inversely with severity of ABA during ABA2

The level of GLT-1 immunoreactivity varied widely among the seven animals that underwent ABA1 and ABA2 and whose brains were processed for EM-ICC. Two of them exhibited no GLT-1 immunoreactivity within the presynaptic terminals of excitatory synapses. In order to assess whether these differences related to their behavior, Pearson correlation analyses were conducted. This test revealed a highly significant negative correlation between GLT-1 immunoreactivity within presynaptic terminals (plasmalemmal plus intracellular) and FRER during ABA2 (Figure 5c, $p = .017$, $R = -.844$).

GLT-1 immunoreactivity at synaptically associated astrocytic processes also varied across animals, ranging from 1.6 to 4.6 per area of synaptic neuropil in stratum radiatum occupied by 100 excitatory axo-spinous synapses. The correlation between GLT-1 levels in these astrocytic processes and each animal's FRER during ABA2 was highly significant and negative (Figure 5d, $p = .038$, $R = -.781$ for plasmalemmal GLT-1).

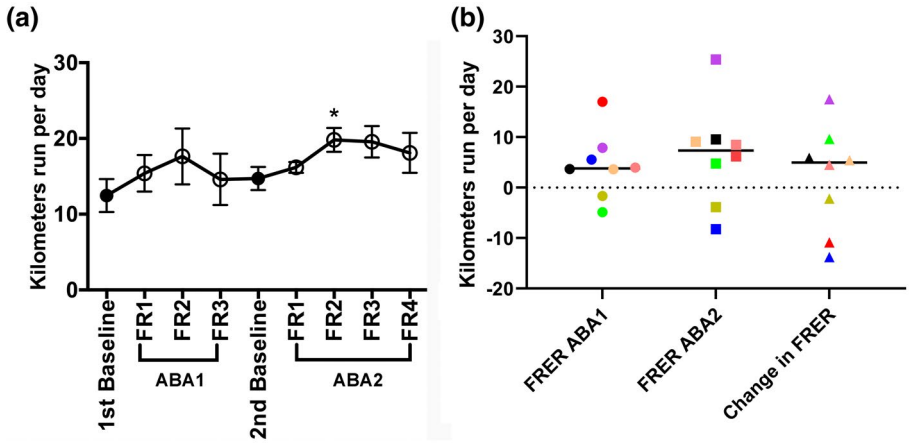

FIGURE 4 FRER during ABA1 and ABA2. (a) Daily values of group averages of wheel running, in kilometers run per day. Error bars indicate *SEM*. Group-averaged FRER is apparent and is significantly greater than baseline for ABA2 but not ABA1 (asterisk depicts $p < .05$). (b) FRER was calculated as the difference in daily averages of wheel running during the food restriction days, relative to the average of the two baseline days immediately prior to ABA. Each data point reflects the averaged value of one individual, with data for each animal color-coded across the three FRER measurements. FRER varies widely across individuals, with six out of the eight subjects increasing wheel running during ABA1 and ABA2, as indicated by the positive values of the kilometers run per day and different levels of ABA vulnerability. Change in FRER, which measured differences in FRER during ABA1 relative to FRER during ABA2, indicates that three out of the eight individuals decreased their FRER during ABA2, compared to their FRER values during ABA1, reflecting a gain of resilience

Astrocytic processes lacking apparent associations with excitatory axo-spinous synapses within the plane of the ultrathin section also exhibited strong correlations in their levels of GLT-1 and change in FRER during ABA2, relative to FRER during ABA1 (Figure 5e, $p = .016$, $R = -.849$ for plasmalemmal SIGs; $p = .012$, $R = -.865$ for the combined counts of SIG at plasma membranes plus intracellular locations).

Comparison of the GLT-1 immunoreactivity across the three subcellular domains reveals that the relative GLT-1 levels are not characteristics that are consistent for individual animals. For example, one animal (Figure 5, red data points) exhibited relatively low levels of GLT-1 immunoreactivity in presynaptic axon terminals and astrocytic processes adjacent to synapses (Figure 5c, 5d), but relatively high GLT-1 levels within astrocytic processes removed from synapses (Figure 5e). Another animal (blue data points) exhibited consistently high levels of GLT-1 across all three subcellular domains. The lack of presynaptic GLT-1 in two animals (orange and red data points) does not necessarily reflect a failure of the immunocytochemical procedure, since other tissue processed in parallel showed robust axonal immunolabeling and the same tissue that exhibited low levels of immunoreactivity within the axon terminals exhibited relatively high levels of GLT-1 immunoreactivity elsewhere.

These negative correlations indicate that the animals with relatively higher expressions of GLT-1 in the vicinity of excitatory axo-spinous synapses exhibited relatively lower ABA severity, quantified as FRER during ABA2 or a change in FRER from ABA1 to ABA2 (Figure 5).

Besides hyperactivity, one of the most prominent symptoms of AN is severe weight loss. We sought to assess whether individual differences in weight loss also correlate with GLT-1 immunoreactivity in the mouse model of ABA. ABA severity, measured as weight loss between the 2nd and 3rd day of the food restriction of ABA2, correlated negatively with presynaptic levels of GLT-1 at intracellular sites ($p = .018$, $R = -.839$) and at the plasma membrane ($p = .047$, $R = -.761$). The weight loss between the 3rd and 4th day of the food restriction of ABA2 did not correlate with presynaptic levels of GLT-1, presumably because some other cellular mechanism dominated the weight change during this period.

3.5 | GLT-1 immunoreactivity correlates with GluN2B-subunit immunoreactivity at excitatory axo-spinous synapses

GLT-1 has been shown to play a significant role in modulating the tonic GluN2B-NMDAR activation by regulating the levels of ambient glutamate (Miller et al., 2014). To determine whether individual differences in GLT-1 levels relates to the neuropil's prevalence of synapses with GluN2B-NMDARs, vibratome sections sampled near the ones analyzed for GLT-1 immunoreactivity were immunolabeled for the GluN2B subunits.

Analysis of this tissue revealed that the association of GluN2B-immunoreactivity with axo-spinous synapses varied widely across individual animals, ranging from 19% to 29% of randomly encountered spines. Of the spines exhibiting GluN2B-subunit immunoreactivity, about half exhibited the immunoreactivity precisely at the synaptic cleft (Figure 2b) or at PSDs (Figure 2e). The levels of GluN2B immunoreactivity

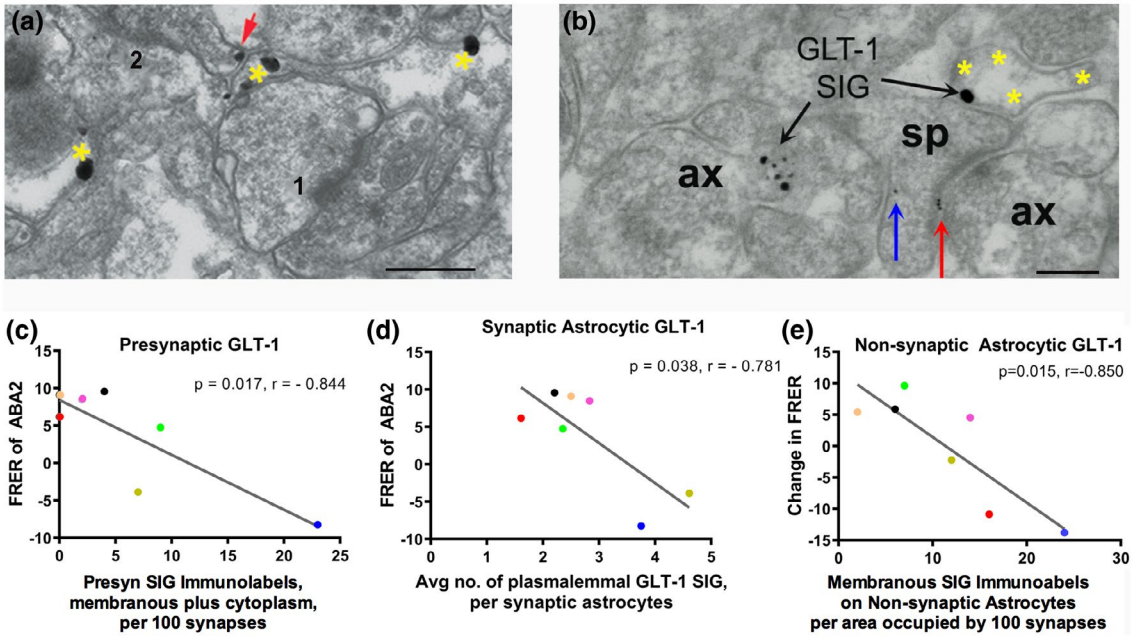

FIGURE 5 Relationships between GLT-1 at excitatory synapses of the HPC and ABA vulnerability. (a) and (b) Electron micrographs depict examples of GLT-1 immunoreactivity in the stratum radiatum of CA1, detected by silver-intensified gold (SIG) as immunolabels. (a) SIG particles along the plasma membrane of astrocytic processes are demarked by yellow asterisks. The red arrow points to an example of SIG within an axon terminal cytoplasm that is presynaptic to the synapse labeled 2. Astrocytic processes form an irregular contour, tightly surrounding the synapses 1 and 2, identified by their dark postsynaptic densities. These astrocytic processes are adjacent to both the presynaptic and postsynaptic neuronal processes. Astrocytic processes also protrude into the sides of the synaptic cleft. (b) This electron micrograph was taken from tissue immunolabeled dually for GLT-1 and GluN2B. GLT-1 immunoreactivity is detectable by the SIG (black arrows), while GluN2B is detectable by the PEG. The red arrow points to GluN2B at the synaptic cleft and over the PSD, whereas the blue arrow points to GluN2B within the dendritic spine cytoplasm. Note that from the leftmost cluster of SIGs, GLT-1 immunoreactivity occurswithin an axon terminal (ax), at the plasma membrane (the two larger SIG particles), and intracellularly (the four smaller SIG particles), whereas the large SIG particle on the right indicates GLT-1 immunoreactivity along the plasma membrane of an astrocytic process (yellow asterisks), identifiable based on the convex contour. Calibration bars equal 200 nm. (c), (d), and (e) Pearson correlation analyses of the relationship between ABA vulnerability(measurements based on FRER)and the levels of GLT1-1 immunoreactivity in:(c) the presynaptic axon terminal, (d) peri-synaptic astrocytic processes, and (e) astrocytic processes without apparent synaptic relationships with excitatory synapses within the ultrathin plane of section. GLT-1 at all three types of locations correlated negatively with FRER. The data points are color-coded to represent animal identification, using the same color scheme shown in Figure 4

per synapse, measured as the number of PEG particles encountered, also varied across synapses. The levels of GLT-1 along the plasma membrane of **astrocytic processes** associated with the excitatory axo-spinous synapses correlated strongly and positively with the total number of GluN2B PEG particles encountered anywhere near the dendritic spine (including at the synaptic cleft, at or near PSDs, along the extrajunctional plasma membrane, or within the cytoplasm of spines) (Figure 6a, $p = .0375$, $R = .783$). Contributing to this correlation were the particularly strong correlations between GLT-1 levels and GluN2B PEG numbers at the PSD (Figure 6b, ($p = .007$, $R = .894$), and between GLT-1 levels and GluN2B levels within the dendritic spine cytoplasm ($p = .048$, $R = .759$). These positive correlations suggest that the localization of astrocytic GLT-1 at the plasma membrane may be co-regulated with spinous localization of GluN2B-NMDARs.

Correlation analysis revealed additional, strong positive relationships between the prevalence of excitatory synapses with GluN2B subunits at the synaptic cleft and GLT-1 levels along the plasma membrane of **presynaptic axon terminals** (Figure 6c, $p = .007$, $R = .893$). Curiously, the prevalence of synapses with GluN2B subunits near but not at PSDs correlated strongly and negatively with presynaptic membranous expressions of GLT-1 ($p = .013$, $R = -.861$) (Figure 6d, $p = .007$, $R = .893$) and there also was a non-significant but trending negative relationship between the prevalence of excitatory synapses with GluN2B subunits sequestered within dendritic spines and presynaptic membranous GLT-1 ($p = .064$, $R = -.727$).

The GluN2B-subunit immunoreactivity at the synaptic clefts reflects their location precisely at functional sites. Conversely, the GluN2B-subunit immunoreactivity located within spine cytoplasm, both near and far from the PSDs, reflects the pools of GluN2B-containing NMDARs that are likely to be in reserve or destined for turnover. The *positive* correlation between the neuropil's prevalence of synaptic GluN2B and presynaptic GLT-1 suggests GLT-1's participation in dampening GluN2B-NMDAR synaptic activity. The *negative* correlation between the prevalence for sequestered GluN2B-immunoreactivity and presynaptic GLT-1 suggests that GLT-1's removal from the plasma membrane of presynaptic terminals may be co-regulated with trafficking of GluN2B-NMDAR away from synaptic clefts.

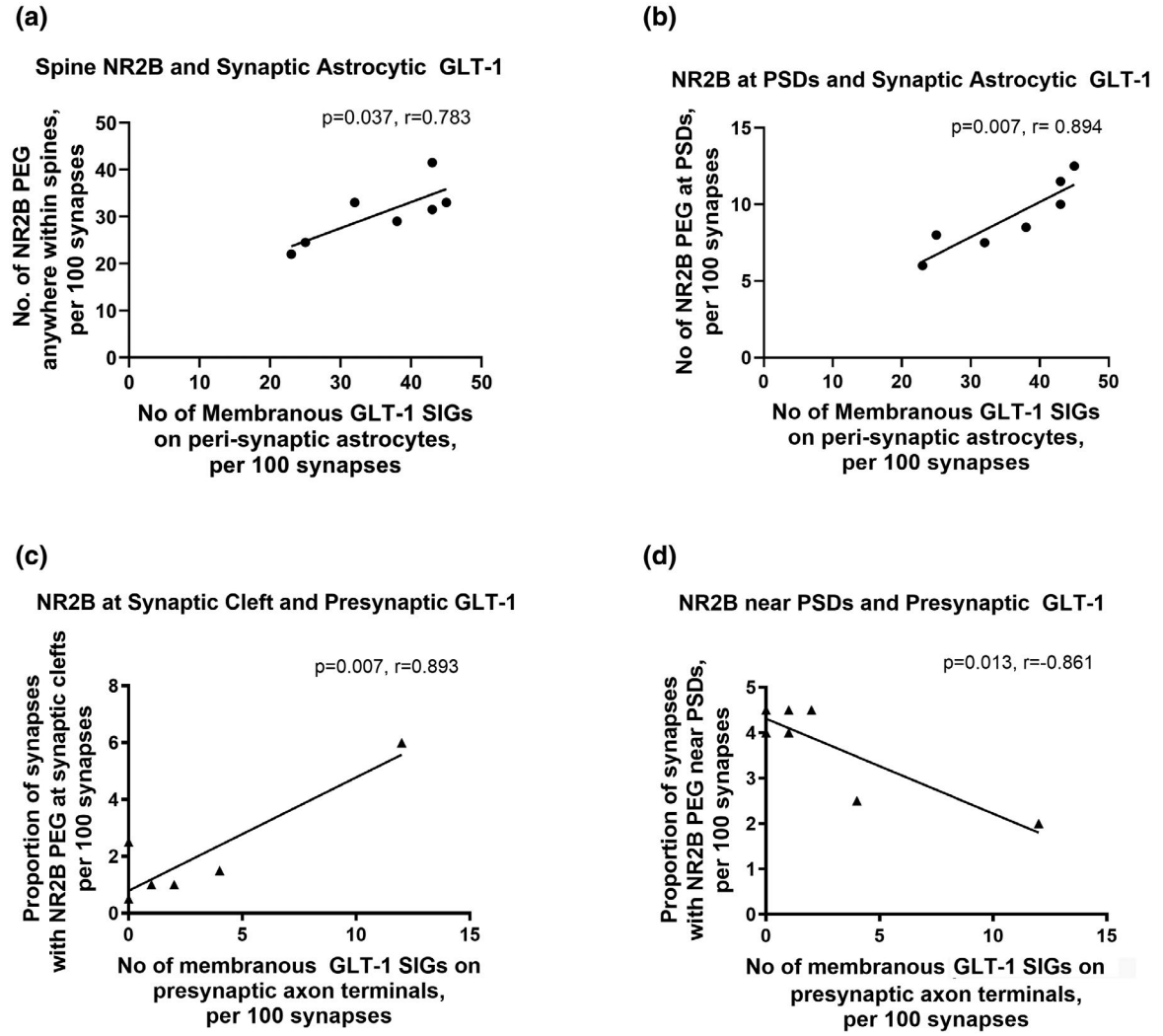

FIGURE 6 Relationships between GluN2B-subunitimmunoreactivity and GLT-1 immunoreactivity at excitatory synapses. Levels of GLT-1 at perisynaptic astrocytes correlate strongly and positively with (a) GluN2B-immunoreactivity at dendritic spines (the number of PEG particles encountered anywhere within dendritic spines), and more precisely at (b) PSDs. Levels of GLT-1 at axon terminals correlate positively with the proportion of synapses with GluN2B-subunits at synaptic clefts (c) but correlate negatively with the proportion of synapses with GluN2B-subunits at sites removed from the PSD (d)

Presynaptic GluN2B-NMDARs have been shown to regulate glutamate release (Dore et al., 2017). We thus assessed whether levels of presynaptic GluN2B-NMDARs correlated with levels of GLT-1 at astrocytic processes or at excitatory axon terminals but found none.

4 | DISCUSSION

Our findings revealed that levels of GLT-1 expressed at excitatory synapses in the HPC vary widely across individuals and that these levels correlate strongly and negatively with FRER and weight loss, the two measurements we used to quantify the severity of ABA. The negative correlations indicate that animals expressing higher levels of GLT-1 at excitatory synapses are able to minimize the severity of ABA. Moreover, the tightly correlated distribution pattern of GLT-1 and GluN2B subunits at excitatory synapses suggests that GLT-1 reduces ABA severity, in part, through the uptake of ambient glutamate, which preferentially activates GluN2B-NMDARs over GluN2A-NMDARs (Miller et al., 2014).

Using an animal model of AN, we have identified GLT-1 as a putative cellular marker underlying the individual differences in vulnerability to maladaptive behaviors associated with AN and ABA. The maladaptive behavior we found to correlate with the cellular marker GLT-1 is compulsive exercise, a hallmark of AN. It has even been reported that 60% of the patients diagnosed with AN were in pursuit of fitness *before* dieting, suggesting that excessive exercise may be a strong contributing factor leading to the illness (Beumont et al., 1994). Compulsive exercise exacerbates weight loss among individuals diagnosed with AN (Beumont et al., 1994), and this feature is recapitulated well in the ABA

animal model of AN that we used. Ordinary wild-type mice voluntarily engage in wheel running, even in the wild, indicating that wheel running is intrinsically rewarding (Meijer & Robbers, 2014). However, within 24 hr of restricting food access, laboratory animals' wheel running begins to increase and quickly becomes maladaptive, such that the animals continue running even during the limited hours of food availability (Aoki et al., 2017; Chowdhury et al., 2013, 2019; Santiago et al., in press; Smits et al., 2008). Thus, the animals voluntarily food-restrict, which is a behavior most often associated with AN. Importantly, because mice exhibit individual differences in FRER and weight loss, we were able to examine the differences in protein expression at the ultrastructural level to unravel the neurobiological mechanisms that may underlie the differences in AN-associated behavior. Analysis of FRER during ABA1 and ABA2 indicates a potentially bimodal distribution: animals that reduce FRER and a greater number of animals that increases FRER (see Figure 4b). Might there be two distinct mechanisms for reducing versus enhancing FRER? Although this is a possibility, the tight linear correlation between FRER values and GLT-1 levels indicates that GLT-1 is one molecule contributing to changes in both directions. Specifically, the linear correlation indicates that those exhibiting relatively low levels of GLT-1 exhibit high FRER, whereas those that express higher levels of GLT-1 exhibit suppression of FRER.

An earlier study from this lab using the rat ABA model had shown that heightened levels of GluN2B-NMDARs at the postsynaptic membrane correlates with ABA vulnerability, quantified as the extent of weight loss on the fourth day of food restriction to ABA (Chen et al., 2017). This was the finding that motivated us to examine the relationship between GluN2B-NMDAR levels in relation to GLT-1 levels. The current study reveals the subcellular relationships between GluN2B and GLT-1 that are acutely dependent on the precise location of GluN2B subunits, resolvable only by EM-ICC. The sharp contrast in their correlations based on a difference of 10 nm (the thickness of the plasma membrane, with GluN2B PEG at versus near PSDs) suggests that trafficking of GluN2B-NMDARs from the reserve pool to active sites on plasma membrane surfaces (McIlhinney et al., 2003) is coordinated with trafficking of presynaptic GLT-1. The tight correlation between GluN2B-subunit PEG at PSDs and facing the synaptic cleft (Figure 6b,c) with synaptic astrocytic GLT-1 suggests that synaptic currents carried by GluN2B-containing NMDARs are strongly regulated by GLT-1 uptake of glutamate into astrocytes, which would dampen synaptic NMDAR currents. Conversely, the strong negative correlation between intracellular pools of GluN2B subunits ("near PSDs" in Figure 6d) and membranous GLT-1 on presynaptic terminals suggests that the sequestration of GluN2B-NMDARs away from the synapses, which is an alternative mechanism to dampen synaptic NMDAR current, may also be coordinated with trafficking of GLT-1 to the plasma membrane of glutamatergic terminals at synapses. Whether such trafficking occurs slowly over days when animals experience the chronic stress of food restriction or quickly enough to modulate synaptic activity concurrent with these stressful events is an interesting question reserved for future studies.

Our EM analysis was restricted to single sections, rather than serially collected sections. This approach enabled us to survey the neuropil widely but precluded addressing certain questions. For example, we were unable to assess whether synapses lacking PSD labeling for GluN2B-NMDAR within a section might express the GluN2B-subunit in the same PSD if the section were cut at another focal plane. Another question that we could not address is whether the heterogeneity of astrocytic and axon terminal labeling for GLT-1 or GluN2B-NMDAR at synapses reflects the heterogeneity in the protein's expression across populations of cells or across subcellular domains of single cells. Answers to these questions may not be critical if we consider that synapses, neurons, and astrocytes operate as flexible ensembles. Furthermore, previous studies comparing serially collected ultrathin sections versus a wider field of single sections concluded that the ultrastructural and morphometric features revealed by the two contrasting approaches are indistinguishable (Seguela et al., 1990; Umbriaco et al., 1994). Serially collected ultrathin sections, as described in a more recent methods paper (Shahidi et al., 2015) will enable one to assess the co-existence of a greatly expanded number of antigens within single synapses. Such experiments are planned for the future, to study the relationship between GLT-1, AMPA receptors, and GluN2A-containing NMDARs.

Whether the correlations revealed in the current study are specific to the HPC or may be generalizable across multiple brain regions is another important question for the future, especially since our previous EM analyses have revealed that the excitability of pyramidal neurons in the prefrontal cortex (Chen et al., 2016; Santiago et al., in press) and amygdala (Wable et al., 2014) are also altered by ABA induction through changes in GABAergic innervations and $GABA_A$ receptor expression levels. In the meantime, it would be worthwhile to explore whether the drugs that are known to boost GLT-1 expression, such as the FDA-approved β-lactam antibiotics, can ameliorate ABA vulnerability to FRER and exacerbated weight loss. Ceftriaxone is one of the β-lactam antibiotics that can be administered systemically to yield concentrations within the brain that are sufficiently high to increase GLT-1 protein expression threefold (Rothstein et al., 2005). Future studies will investigate the potentially ameliorative properties of ceftriaxone in ABA.

ACKNOWLEDGMENTS

The study was made possible through the following grants: NIH Grant R21MH105846, Klarman Family Foundation Grant Program in Eating Disorders Research, P30 EY13079, New York University Research Challenge Fund, NSF-REU, and The Vulnerable Brain Project. We thank Vladlena Lee and Victoria Dreyer for their assistance with the GluN2B-immunocytochemistry procedure during the summer of 2017. We thank Rose Temizer, Cenk Akiz, Emily Makowicz, Ikponmwosa Pat-Osagie, and Jennifer Li for their assistance in recording body weight data of adolescent mice.

CONFLICT OF INTEREST

None of the authors have any conflict of interest to disclose.

DATA AVAILABILITY STATEMENT

The data that support the findings of this study are available from the corresponding author upon reasonable request.

ORCID

Chiye Aoki https://orcid.org/0000-0003-4010-9425

REFERENCES

Adams, M. M., Shah, R. A., Janssen, W. G., & Morrison, J. H. (2001). Different modes of hippocampal plasticity in response to estrogen in young and aged female rats. *Proceedings of the National Academy of Sciences of the United States of America*, *98*(14), 8071–8076. https://doi.org/10.1073/pnas.141215898

Aoki, C., Chowdhury, T. G., Wable, G. S., & Chen, Y. W. (2017). Synaptic changes in the hippocampus of adolescent female rodents associated with resilience to anxiety and suppression of food restriction-evoked hyperactivity in an animal model for anorexia nervosa. *Brain Research*, *1654*(Pt B), 102–115. https://doi.org/10.1016/j.brainres.2016.01.019

Aoki, C., Fujisawa, S., Mahadomrongkul, V., Shah, P. J., Nader, K., & Erisir, A. (2003). NMDA receptor blockade in intact adult cortex increases trafficking of NR2A subunits into spines, postsynaptic densities, and axon terminals. *Brain Research*, *963*(1–2), 139–149. https://doi.org/10.1016/S0006-8993(02)03962-8

Aoki, C., Kojima, N., Sabaliauskas, N., Shah, L., Ahmed, T. H., Oakford, J., Ahmed, T., Yamazaki, H., Hanamura, K., & Shirao, T. (2009). Drebrin a knockout eliminates the rapid form of homeostatic synaptic plasticity at excitatory synapses of intact adult cerebral cortex. *The Journal of Comparative Neurology*, *517*(1), 105–121. https://doi.org/10.1002/cne.22137

Aoki, C., Lee, J., Nedelescu, H., Ahmed, T., Ho, A., & Shen, J. (2009). Increased levels of NMDA receptor NR2A subunits at pre- and postsynaptic sites of the hippocampal CA1: An early response to conditional double knockout of presenilin 1 and 2. *The Journal of Comparative Neurology*, *517*(4), 512–523. https://doi.org/10.1002/cne.22151

Aoki, C., Sabaliauskas, N., Chowdhury, T., Min, J. Y., Colacino, A. R., Laurino, K., & Barbarich-Marsteller, N. C. (2012). Adolescent female rats exhibiting activity-based anorexia express elevated levels of GABA(A) receptor alpha4 and delta subunits at the plasma membrane of hippocampal CA1 spines. *Synapse (New York, N. Y.)*, *66*(5), 391–407. https://doi.org/10.1002/syn.21528

Aoki, C., Wable, G., Chowdhury, T. G., Sabaliauskas, N. A., Laurino, K., & Barbarich-Marsteller, N. C. (2014). alpha4betadelta-GABAARs in the hippocampal CA1 as a biomarker for resilience to activity-based anorexia. *Neuroscience*, *265*, 108–123. https://doi.org/10.1016/j.neuroscience.2014.01.011

Arcelus, J., Mitchell, A. J., Wales, J., & Nielsen, S. (2011). Mortality rates in patients with anorexia nervosa and other eating disorders. A meta-analysis of 36 studies. *Archives of General Psychiatry*, *68*(7), 724–731. https://doi.org/10.1001/archgenpsychiatry.2011.74

Barnes, J. R., Mukherjee, B., Rogers, B. C., Nafar, F., Gosse, M., & Parsons, M. P. (2020). The relationship between glutamate dynamics and activity-dependent synaptic plasticity. *Journal of Neuroscience*, *40*(14), 2793–2807. https://doi.org/10.1523/JNEUROSCI.1655-19.2020

Beadle, J. N., Paradiso, S., Brumm, M., Voss, M., Halmi, K., & McCormick, L. M. (2015). Larger hippocampus size in women with anorexia nervosa who exercise excessively than healthy women. *Psychiatry Research*, *232*(2), 193–199. https://doi.org/10.1016/j.pscychresns.2014.10.013

Beschorner, R., Simon, P., Schauer, N., Mittelbronn, M., Schluesener, H. J., Trautmann, K., Dietz, K., & Meyermann, R. (2007). Reactive astrocytes and activated microglial cells express EAAT1, but not EAAT2, reflecting a neuroprotective potential following ischaemia. *Histopathology*, *50*(7), 897–910. https://doi.org/10.1111/j.1365-2559.2007.02703.x

Beumont, P. J., Arthur, B., Russell, J. D., & Touyz, S. W. (1994). Excessive physical activity in dieting disorder patients: Proposals for a supervised exercise program. *International Journal of Eating Disorders*, *15*(1), 21–36. https://doi.org/10.1002/1098-108X(199401)15:1<21:AID-EAT2260150104>3.0.CO;2-K

Birmingham, C. L., Su, J., Hlynsky, J. A., Goldner, E. M., & Gao, M. (2005). The mortality rate from anorexia nervosa. *International Journal of Eating Disorders*, *38*(2), 143–146. https://doi.org/10.1002/eat.20164

Carr, K. D. (2011). Food scarcity, neuroadaptations, and the pathogenic potential of dieting in an unnatural ecology: Binge eating and drug abuse. *Physiology & Behavior*, *104*(1), 162–167. https://doi.org/10.1016/j.physbeh.2011.04.023

Casper, R. C., Sullivan, E. L., & Tecott, L. (2008). Relevance of animal models to human eating disorders and obesity. *Psychopharmacology (Berl)*, *199*(3), 313–329. https://doi.org/10.1007/s00213-008-1102-2

Chen, W., Mahadomrongkul, V., Berger, U. V., Bassan, M., DeSilva, T., Tanaka, K., & Rosenberg, P. A. (2004). The glutamate transporter GLT1a is expressed in excitatory axon terminals of mature hippocampal neurons. *Journal of Neuroscience*, *24*(5), 1136–1148. https://doi.org/10.1523/JNEUROSCI.1586-03.2004

Chen, Y. W., Actor-Engel, H., & Aoki, C. (2018). alpha4-GABAA receptors of hippocampal pyramidal neurons are associated with resilience against activity-based anorexia for adolescent female mice but not for males. *Molecular and Cellular Neurosciences*, *90*, 33–48. https://doi.org/10.1016/j.mcn.2018.04.008

Chen, Y. W., Actor-Engel, H., Sherpa, A. D., Klingensmith, L., Chowdhury, T. G., & Aoki, C. (2017). NR2A- and NR2B-NMDA receptors and drebrin within postsynaptic spines of the hippocampus correlate with hunger-evoked exercise. *Brain Structure and Function*, *222*(5), 2271–2294. https://doi.org/10.1007/s00429-016-1341-7

Chen, Y. W., Akad, A., Aderogba, R., Chowdhury, T. G., & Aoki, C. (2018). Dendrites of the dorsal and ventral hippocampal CA1 pyramidal neurons of singly housed female rats exhibit lamina-specific growths and retractions during adolescence that are responsive to pair housing. *Synapse (New York, N. Y.)*, *72*(7), e22034. https://doi.org/10.1002/syn.22034

Chen, Y. W., Wable, G. S., Chowdhury, T. G., & Aoki, C. (2016). Enlargement of axo-somatic contacts formed by GAD-immunoreactive axon terminals onto layer V pyramidal neurons in the medial prefrontal cortex of adolescent female mice is associated with suppression of food restriction-evoked hyperactivity and resilience to activity-based anorexia. *Cerebral Cortex*, *26*(6), 2574–2589. https://doi.org/10.1093/cercor/bhv087

Chowdhury, T. G., Barbarich-Marsteller, N. C., Chan, T. E., & Aoki, C. (2014). Activity-based anorexia has differential effects on apical dendritic branching in dorsal and ventral hippocampal CA1. *Brain Structure and Function*, *219*(6), 1935–1945. https://doi.org/10.1007/s00429-013-0612-9

Chowdhury, T., Chen, Y.-W., & Aoki, C. (2015). Using the activity-based anorexia rodent model to study the neurobiological basis of anorexia nervosa. *Journal of Visualized Experiments*, *104*, e52927. https://doi.org/10.3791/52927

Chowdhury, T. G., Rios, M. B., Chan, T. E., Cassataro, D. S., Barbarich-Marsteller, N. C., & Aoki, C. (2014). Activity-based anorexia during adolescence disrupts normal development of the CA1 pyramidal cells in the ventral hippocampus of female rats. *Hippocampus*, *24*(12), 1421–1429. https://doi.org/10.1002/hipo.22320

Chowdhury, T. G., Wable, G. S., Chen, Y.-W., Tateyama, K., Yu, I., Wang, J.-Y., Reyes, A. D., & Aoki, C. (2019). Voluntary wheel running exercise evoked by food-restriction stress exacerbates weight loss of adolescent female rats but also promotes resilience by enhancing GABAergic inhibition of pyramidal neurons in the dorsal hippocampus. *Cerebral Cortex*, *29*(10), 4035–4049. https://doi.org/10.1093/cercor/bhy283

Chowdhury, T. G., Wable, G. S., Sabaliauskas, N. A., & Aoki, C. (2013). Adolescent female C57BL/6 mice with vulnerability to activity-based anorexia exhibit weak inhibitory input onto hippocampal CA1 pyramidal cells. *Neuroscience*, *241*, 250–267. https://doi.org/10.1016/j.neuroscience.2013.03.020

Churchill, J. D., Galvez, R., Colcombe, S., Swain, R. A., Kramer, A. F., & Greenough, W. T. (2002). Exercise, experience and the aging brain. *Neurobiology of Aging*, *23*(5), 941–955. https://doi.org/10.1016/s0197-4580(02)00028-3

Danbolt, N. C. (2001). Glutamate uptake. *Progress in Neurobiology*, *65*(1), 1–105. https://doi.org/10.1016/s0301-0082(00)00067-8

Danbolt, N. C., Furness, D. N., & Zhou, Y. (2016). Neuronal vs glial glutamate uptake: Resolving the conundrum. *Neurochemistry International*, *98*, 29–45. https://doi.org/10.1016/j.neuint.2016.05.009

Davis, C., Katzman, D. K., & Kirsh, C. (1999). Compulsive physical activity in adolescents with anorexia nervosa: A psychobehavioral spiral of pathology. *The Journal of Nervous and Mental Disease*, *187*(6), 336–342. https://doi.org/10.1097/00005053-199906000-00002

Dellava, J. E., Thornton, L. M., Hamer, R. M., Strober, M., Plotnicov, K., Klump, K. L., Brandt, H., Crawford, S., Fichter, M. M., Halmi, K. A., Jones, I., Johnson, C., Kaplan, A. S., LaVia, M., Mitchell, J., Rotondo, A., Treasure, J., Woodside, D. B., Berrettini, W. H., … Bulik, C. M. (2010). Childhood anxiety associated with low BMI in women with anorexia nervosa. *Behavior Research and Therapy*, *48*(1), 60–67. https://doi.org/10.1016/j.brat.2009.09.009

Dore, K., Stein, I. S., Brock, J. A., Castillo, P. E., Zito, K., & Sjostrom, P. J. (2017). Unconventional NMDA receptor signaling. *Journal of Neuroscience*, *37*(45), 10800–10807. https://doi.org/10.1523/JNEUROSCI.1825-17.2017

Fanselow, M. S., & Dong, H. W. (2010). Are the dorsal and ventral hippocampus functionally distinct structures? *Neuron*, *65*(1), 7–19. https://doi.org/10.1016/j.neuron.2009.11.031

Fujisawa, S., & Aoki, C. (2003). In vivo blockade of N-methyl-D-aspartate receptors induces rapid trafficking of NR2B subunits away from synapses and out of spines and terminals in adult cortex. *Neuroscience*, *121*(1), 51–63. https://doi.org/10.1016/S0306-4522(03)00341-5

Girbovan, C., Kent, P., Merali, Z., & Plamondon, H. (2016). Dose-related effects of chronic resveratrol administration on neurogenesis, angiogenesis, and corticosterone secretion are associated with improved spatial memory retention following global cerebral ischemia. *Nutritional Neuroscience*, *19*(8), 352–368. https://doi.org/10.1179/1476830515Y.0000000020

Goddings, A. L., Mills, K. L., Clasen, L. S., Giedd, J. N., Viner, R. M., & Blakemore, S. J. (2014). The influence of puberty on subcortical brain development. *NeuroImage*, *88*, 242–251. https://doi.org/10.1016/j.neuroimage.2013.09.073

Greenwood, B. N., & Fleshner, M. (2008). Exercise, learned helplessness, and the stress-resistant brain. *NeuroMolecular Medicine*, *10*(2), 81–98. https://doi.org/10.1007/s12017-008-8029-y

Gutierrez, E. (2013). A rat in the labyrinth of anorexia nervosa: Contributions of the activity-based anorexia rodent model to the understanding of anorexia nervosa. *International Journal of Eating Disorders*, *46*(4), 289–301. https://doi.org/10.1002/eat.22095

He, Y., Janssen, W. G., & Morrison, J. H. (1998). Synaptic coexistence of AMPA and NMDA receptors in the rat hippocampus: A postembedding immunogold study. *Journal of Neuroscience Research*, *54*(4), 444–449. https://doi.org/10.1002/(SICI)1097-4547(19981115)54:4<444:AID-JNR2>3.0.CO;2-3

Hebebrand, J., Exner, C., Hebebrand, K., Holtkamp, C., Casper, R. C., Remschmidt, H., Herpertz-Dahlmann, B., & Klingenspor, M. (2003). Hyperactivity in patients with anorexia nervosa and in semistarved rats: Evidence for a pivotal role of hypoleptinemia. *Physiology & Behavior*, *79*(1), 25–37. https://doi.org/10.1016/S0031-9384(03)00102-1

Hermens, D. F., Simcock, G., Dutton, M., Boucas, A. P., Can, A. T., Lilley, C., & Lagopoulos, J. (2020). Anorexia nervosa, zinc deficiency and the glutamate system: The ketamine option. *Progress in Neuro-Psychopharmacology and Biological Psychiatry*, *101*, 109921. https://doi.org/10.1016/j.pnpbp.2020.109921

Huttunen, P., & Myers, R. D. (1986). Tetrahydro-beta-carboline micro-injected into the hippocampus induces an anxiety-like state in the rat. *Pharmacology, Biochemistry and Behavior*, *24*(6), 1733–1738.

Kanarek, R. B., D'Anci, K. E., Jurdak, N., & Mathes, W. F. (2009). Running and addiction: Precipitated withdrawal in a rat model of activity-based anorexia. *Behavioral Neuroscience*, *123*(4), 905–912. https://doi.org/10.1037/a0015896

Kataoka, Y., Shibata, K., Miyazaki, A., Inoue, Y., Tominaga, K., Koizumi, S., Ueki, S., & Niwa, M. (1991). Involvement of the dorsal hippocampus in mediation of the antianxiety action of tandospirone, a 5-hydroxytryptamine1A agonistic anxiolytic. *Neuropharmacology*, *30*(5), 475–480. https://doi.org/10.1016/0028-3908(91)90009-Z

Kaye, W. H., Bulik, C. M., Thornton, L., Barbarich, N., & Masters, K. (2004). Comorbidity of anxiety disorders with anorexia and bulimia nervosa. *American Journal of Psychiatry*, *161*(12), 2215–2221. https://doi.org/10.1176/appi.ajp.161.12.2215

Knackstedt, L. A., Melendez, R. I., & Kalivas, P. W. (2010). Ceftriaxone restores glutamate homeostasis and prevents relapse to cocaine seeking. *Biological Psychiatry*, *67*(1), 81–84. https://doi.org/10.1016/j.biopsych.2009.07.018

Kron, L., Katz, J. L., Gorzynski, G., & Weiner, H. (1978). Hyperactivity in anorexia nervosa: A fundamental clinical feature. *Comprehensive Psychiatry*, *19*(5), 433–440. https://doi.org/10.1016/0010-440X(78)90072-X

Kronenberger, J. P., & Medioni, J. (1985). Food neophobia in wild and laboratory mice (Mus musculus domesticus). *Behavioural Processes*, *11*(1), 53–59. https://doi.org/10.1016/0376-6357(85)90102-0

McIlhinney, R. A., Philipps, E., Le Bourdelles, B., Grimwood, S., Wafford, K., Sandhu, S., & Whiting, P. (2003). Assembly of N-methyl-D-aspartate (NMDA) receptors. *Biochemical Society Transactions*, *31*(Pt 4), 865–868. https://doi.org/10.1042/bst0310865

Mehl, M. L., Schott, H. C., 2nd, Sarkar, D. K., & Bayly, W. M. (2000). Effects of exercise intensity and duration on plasma beta-endorphin concentrations in horses. *American Journal of Veterinary Research*, *61*(8), 969–973. https://doi.org/10.2460/ajvr.2000.61.969

Meijer, J. H., & Robbers, Y. (2014). Wheel running in the wild. *Proceedings of the Royal Society B: Biological Sciences*, *281*(1786), 20140210. https://doi.org/10.1098/rspb.2014.0210

Miller, O. H., Yang, L., Wang, C. C., Hargroder, E. A., Zhang, Y., Delpire, E., & Hall, B. J. (2014). GluN2B-containing NMDA receptors regulate depression-like behavior and are critical for the rapid antidepressant actions of ketamine. *Elife*, *3*, e03581. https://doi.org/10.7554/eLife.03581

Mills, K. L., Goddings, A. L., Clasen, L. S., Giedd, J. N., & Blakemore, S. J. (2014). The developmental mismatch in structural brain maturation during adolescence. *Developmental Neuroscience*, *36*(3–4), 147–160. https://doi.org/10.1159/000362328

Paluska, S. A., & Schwenk, T. L. (2000). Physical activity and mental health: Current concepts. *Sports Medicine (Auckland, N. Z.)*, *29*(3), 167–180. https://doi.org/10.2165/00007256-200029030-00003

Petr, G. T., Sun, Y., Frederick, N. M., Zhou, Y., Dhamne, S. C., Hameed, M. Q., Miranda, C., Bedoya, E. A., Fischer, K. D., Armsen, W., Wang, J., Danbolt, N. C., Rotenberg, A., Aoki, C. J., & Rosenberg, P. A. (2015). Conditional deletion of the glutamate transporter GLT-1 reveals that astrocytic GLT-1 protects against fatal epilepsy while neuronal GLT-1 contributes significantly to glutamate uptake into synaptosomes. *Journal of Neuroscience*, *35*(13), 5187–5201. https://doi.org/10.1523/JNEUROSCI.4255-14.2015

Peters, A., Palay, S. L., & Webster, Hd (1991). *The fine structure of the nervous system: Neurons and their supporting cells* (3rd ed.). New York: Oxford University.

Phend, K. D., Rustioni, A., & Weinberg, R. J. (1995). An osmium-free method of epon embedment that preserves both ultrastructure and antigenicity for post-embedding immunocytochemistry. *Journal of Histochemistry and Cytochemistry*, *43*(3), 283–292. https://doi.org/10.1177/43.3.7532656

Rinaldi, T., Kulangara, K., Antoniello, K., & Markram, H. (2007). Elevated NMDA receptor levels and enhanced postsynaptic long-term potentiation induced by prenatal exposure to valproic acid. *Proceedings of the National Academy of Sciences of the United States of America*, *104*(33), 13501–13506. https://doi.org/10.1073/pnas.0704391104

Rothstein, J. D., Dykes-Hoberg, M., Pardo, C. A., Bristol, L. A., Jin, L., Kuncl, R. W., Kanai, Y., Hediger, M. A., Wang, Y., Schielke, J. P., & Welty, D. F. (1996). Knockout of glutamate transporters reveals a major role for astroglial transport in excitotoxicity and clearance of glutamate. *Neuron*, *16*(3), 675–686. https://doi.org/10.1016/s0896-6273(00)80086-0

Rothstein, J. D., Patel, S., Regan, M. R., Haenggeli, C., Huang, Y. H., Bergles, D. E., & Fisher, P. B. (2005). Beta-lactam antibiotics offer neuroprotection by increasing glutamate transporter expression. *Nature*, *433*(7021), 73–77. https://doi.org/10.1038/nature03180

Santiago, A. N., Makowicz, E. A., Du, M., & Aoki, C. (in press). Food restriction engages prefrontal corticostriatal cells and local microcircuitry to drive the decision to run versus conserve energy. *Cerebral Cortex*. https://doi.org/10.1093/cercor/bhaa394

Seguela, P., Watkins, K. C., Geffard, M., & Descarries, L. (1990). Noradrenaline axon terminals in adult rat neocortex: An immunocytochemical analysis in serial thin sections. *Neuroscience*, *35*(2), 249–264. https://doi.org/10.1016/0306-4522(90)90079-j

Services, U. D. o. H. a. H. (1998). *Clinician's handbook of preventive services: Put prevention into practice* (2nd ed.). International Medical Publishing.

Shahidi, R., Williams, E. A., Conzelmann, M., Asadulina, A., Verasztó, C., Jasek, S., Bezares-Calderón, L. A., & Jékely, G. (2015). A serial multiplex immunogold labeling method for identifying peptidergic neurons in connectomes. *Elife*, *4*. https://doi.org/10.7554/eLife.11147

Shen, H., Gong, Q. H., Aoki, C., Yuan, M., Ruderman, Y., Dattilo, M., & Smith, S. S. (2007). Reversal of neurosteroid effects at alpha4beta2delta GABAA receptors triggers anxiety at puberty. *Nature Neuroscience*, *10*(4), 469–477.

Shen, H., Sabaliauskas, N., Sherpa, A., Fenton, A. A., Stelzer, A., Aoki, C., & Smith, S. S. (2010). A critical role for alpha4betadelta GABAA receptors in shaping learning deficits at puberty in mice. *Science*, *327*(5972), 1515–1518.

Smith, M. A., & Lyle, M. A. (2006). Chronic exercise decreases sensitivity to mu opioids in female rats: Correlation with exercise output. *Pharmacology, Biochemistry and Behavior*, *85*(1), 12–22. https://doi.org/10.1016/j.pbb.2006.06.020

Smits, J. A., Berry, A. C., Rosenfield, D., Powers, M. B., Behar, E., & Otto, M. W. (2008). Reducing anxiety sensitivity with exercise. *Depress Anxiety*, *25*(8), 689–699. https://doi.org/10.1002/da.20411

Sullivan, P. F. (1995). Mortality in anorexia nervosa. *American Journal of Psychiatry*, *152*(7), 1073–1074.

Talaenko, A. N. (1993). The Neurochemical profiles of the dorsal hippocampus and the antiaversive effects of anxiolytics in different models of anxiety in rats. *The Journal of Nervous and Mental Disease*, *43*, 621–626.

Thornton, L. M., Dellava, J. E., Root, T. L., Lichtenstein, P., & Bulik, C. M. (2011). Anorexia nervosa and generalized anxiety disorder: Further explorations of the relation between anxiety and body mass index. *Journal of Anxiety Disorders*, *25*(5), 727–730. https://doi.org/10.1016/j.janxdis.2011.03.010

Umbriaco, D., Watkins, K. C., Descarries, L., Cozzari, C., & Hartman, B. K. (1994). Ultrastructural and morphometric features of the acetylcholine innervation in adult rat parietal cortex: An electron microscopic study in serial sections. *The Journal of Comparative Neurology*, *348*(3), 351–373. https://doi.org/10.1002/cne.903480304

Ventura, R., & Harris, K. M. (1999). Three-dimensional relationships between hippocampal synapses and astrocytes. *Journal of Neuroscience*, *19*(16), 6897–6906. https://doi.org/10.1523/JNEUROSCI.19-16-06897.1999

Wable, G. S., Barbarich-Marsteller, N. C., Chowdhury, T. G., Sabaliauskas, N. A., Farb, C. R., & Aoki, C. (2014). Excitatory synapses on dendritic shafts of the caudal basal amygdala exhibit elevated levels of GABAA receptor alpha4 subunits following the induction of activity-based anorexia. *Synapse (New York, N. Y.)*, *68*(1), 1–15. https://doi.org/10.1002/syn.21690

Wable, G. S., Min, J. Y., Chen, Y. W., & Aoki, C. (2015). Anxiety is correlated with running in adolescent female mice undergoing activity-based anorexia. *Behavioral Neuroscience*, *129*(2), 170–182. https://doi.org/10.1037/bne0000040

Watson, H. J., Yilmaz, Z., Thornton, L. M., Hübel, C., Coleman, J. R. I., Gaspar, H. A., Bryois, J., Hinney, A., Leppä, V. M., Mattheisen, M., Medland, S. E., Ripke, S., Yao, S., Giusti-Rodríguez, P., Hanscombe, K. B., Purves, K. L., Adan, R. A. H., Alfredsson, L., Ando, T., … Bulik, C. M. (2019). Genome-wide association study identifies eight risk loci and implicates metabo-psychiatric origins for anorexia nervosa. *Nature Genetics*, *51*(8), 1207–1214. https://doi.org/10.1038/s41588-019-0439-2

Zunker, C., Mitchell, J. E., & Wonderlich, S. A. (2011). Exercise interventions for women with anorexia nervosa: A review of the literature. *International Journal of Eating Disorders*, *44*(7), 579–584. https://doi.org/10.1002/eat.20862

How to cite this article: Bilash OM, Actor-Engel HS, Sherpa AD, Chen Y-W, Aoki C. Suppression of food restriction-evoked hyperactivity in activity-based anorexia animal model through glutamate transporters GLT-1 at excitatory synapses in the hippocampus. *Synapse*. 2021;75:e22197. https://doi.org/10.1002/syn.22197